Appl. Phys. B 70, 607–620 (2000) / Digital Object Identifier (DOI) 10.1007/s003409900168

Applied Physics B
Lasers
and Optics

Temperature and concentration measurements in acetylene-nitrogen mixtures in the range 300–600 K using dual-broadband rotational CARS

J. Bood, P.-E. Bengtsson, M. Aldén

Department of Combustion Physics, Lund Institute of Technology, P.O. Box 118, S-221 00 Lund, Sweden
(Fax: +46-46/222-4542, E-mail: joakim.bood@forbrf.lth.se)

Received: 8 June 1999/Revised version: 3 Spetember 1999/Published online: 3 November 1999

Abstract. Pure rotational coherent anti-Stokes Raman scattering (CARS) experiments have been performed in acetylene for temperatures ranging from 294 to 582 K, and in mixtures of acetylene and nitrogen in the mole fraction range of 0.06–0.32 for acetylene at room temperature. The experimental spectra are evaluated by a least-square fitting to libraries of theoretically calculated spectra using two different Raman linewidth models, one with and one without dependence on the rotational quantum number J. It is found that a J-dependent model is favourable, both regarding temperature measurements in pure acetylene, and simultaneous acetylene concentration and temperature measurements in different mixtures of acetylene and nitrogen. For the temperature measurements performed in pure acetylene the temperature inaccuracy is generally less than 2% when the J-dependent model for the Raman linewidths is used. It is found that fitting the value of the non-resonant susceptibility significantly improves the quality of the spectral fits and is a requirement for high temperature accuracy with the present model. The evaluated concentrations show a maximum error of 13% on a relative scale. Potential sources of systematical errors both regarding measured temperatures and acetylene concentrations are discussed.

PACS: 33.15; 42.65

Coherent anti-Stokes Raman spectroscopy (CARS) is today a widely used method for non-intrusive gas-phase thermometry in combustion research [1–3]. Most previous work on CARS has been on vibrational CARS, where the signal originates from transitions between rotational levels in different vibrational states. The temperature dependence of the spectral shape is mainly due to the temperature-dependent population distribution of the rovibrational states, between which the transitions occur. Normally, the spectrum of nitrogen is recorded, since nitrogen is inert and occurs in high concentrations in air-fed combustion processes. Vibrational CARS has its strongest temperature-sensitivity when excited vibrational states are significantly populated, manifested by a so-called hot band in the spectrum, which for nitrogen occurs at temperatures above ≈ 1000 K.

Concentration measurement using vibrational CARS is mainly based on either analysis of the spectral shape or on the ratio of the integrated spectral intensity of two species [3]. At low and moderate concentrations, normally 0.5%–25%, the spectral synthesis of the resonant and the non-resonant susceptibility provides concentration-sensitive spectral shapes. If the concentration is higher, the resonant susceptibility will strongly dominate the spectral signature, and if it is lower the resonant contribution will drown in the non-resonant background, in both cases resulting in a poor spectral sensitivity on concentration. Moreover, this approach requires accurate knowledge of the value of the non-resonant susceptibility, which is dependent on the present composition of the mixture.

Concentration measurements of more than one species at a time is for most species not possible by vibrational CARS, since the vibrational resonances of the different species normally are spectrally too far apart to be excited by a single broadband dye laser. However, an important exception in this context is acetylene/nitrogen [4, 5], other exceptions are N_2/CO [6] and CO_2/O_2 [7]. High-resolution scanning vibrational CARS measurements of acetylene in a CH_4/C_2H_2/air flame have been reported by Lucht et al. [5]. In this work acetylene temperature and concentration measurements were performed using a two-channel, in situ referencing system [8, 9] where the resonant and non-resonant signals are separated in two different channels. Several techniques involving two dye lasers have been used for measurements of concentration ratios, for example the dual-broadband vibrational CARS technique [10], the dual-Stokes approach [11], and the dual-pump technique [12].

In pure rotational CARS, the method applied in the present study, the Raman transitions occur between rotational level J and $J+2$ (S-branch) within the same vibrational state. In vibrational CARS, on the contrary, the Raman transitions occur between rotational levels of same J number (Q-branch) belonging to different vibrational states. Thus, the spectral lines of a rotational CARS spectrum are, in contrast to a vibrational CARS spectrum, well separated. This is

advantageous when measurements at high pressures are performed, since the spectral lines remain isolated up to at least 5 MPa, i.e. no pressure collisional narrowing effects have to be considered. Another benefit of rotational CARS thermometry is that the evaluated temperature has a weak dependence on the non-resonant susceptibility and the slit width for conditions typical in combustion processes [13, 14]. Moreover, rotational CARS can be applied in at least moderately sooting flames [15, 16], which is generally not the case for vibrational CARS, since the spectra will suffer from interferences due to laser-produced C_2-radicals which can introduce significant errors in the evaluated temperatures [17]. In the present work a variant called dual-broadband rotational CARS is used [18, 19]. Dual-broadband rotational CARS is nowadays a well-established method for thermometry in combustion research, and has for instance been applied for combustion engine diagnostics [20, 21].

In contrast to vibrational CARS, a rotational CARS spectrum contains spectral lines from almost all molecules in the sample (the perhaps most important exception is H_2), on condition that the present molecules are rotational Raman active. The reason for this is simply because the rotational energy levels are much more closely separated than the vibrational levels. Hence, a large number of rotational resonances of various molecules can be covered within the spectral width of a single dye-laser profile. Therefore, rotational CARS has the potential for simultaneous temperature and multiple species concentration measurements. Since nitrogen and oxygen are diatomic molecules with well-known molecular data, most work has so far been on concentration measurements of these species. Simultaneous measurements of temperature and relative oxygen-to-nitrogen concentrations have been demonstrated in many different temperature intervals from room temperature up to flame temperatures [22–26]. Applied measurements of oxygen concentrations have been carried out by Black and Long [27] and by Bengtsson et al. [20].

Since diatomic molecules are comparatively small, their rotational and vibrational structure is relatively simple. The molecular complexity rapidly increases as the size of the molecule increases, especially if the molecule in addition is bent. However, rotational CARS spectra of some polyatomic molecules such as ethylene and sulphur dioxide have been calculated [28]. Recently Schenk et al. [29] performed simultaneous temperature and relative nitrogen-to-carbon dioxide concentration measurements at low temperatures (up to 773 K). Their results on pure carbon dioxide show excellent agreement between CARS and thermocouple measurements, and the accuracy of the evaluated relative carbon dioxide concentrations is good.

In a previous work by Bengtsson et al. [30] it was found that acetylene gives rise to strong peaks in rotational CARS spectra recorded in different mixtures of acetylene and air, and a good potential for relative acetylene concentration measurements using dual-broadband rotational CARS was predicted. In the present paper, acetylene temperatures and relative acetylene-to-nitrogen concentrations measured by dual-broadband rotational CARS are for the first time reported. Measurements are performed in both pure acetylene, at six different temperatures ranging from 294 to 582 K, and in seven different mixtures of acetylene and nitrogen with mole fractions of acetylene of 0.06–0.32 .

In Sect. 1 the fundamental molecular properties of acetylene are presented, and in Sect. 2 experimental details and measurements are described. The procedure for spectral evaluation is outlined in Sect. 3, after which the results are presented in Sect. 4. The results are discussed and summarized in Sect. 5 and 6, respectively.

1 Molecular structure of acetylene

Acetylene is a linear and symmetric molecule belonging to the point group $D_{\infty h}$. Since the rotational Raman cross section is proportional to the polarizability anisotropy, linear molecules have strong rotational Raman cross-sections. Hence, a rotational CARS spectrum of acetylene shows strong spectral lines.

In Fig. 1 rotational CARS spectra of acetylene are compared with nitrogen spectra for three different temperatures. The most obvious differences between the acetylene and nitrogen spectra are the separations of the spectral lines due to the different rotational constants (*B*-constants), and the alternations of the line intensities due to different nuclear spin statistics. It is apparent that the intensity ratio between neighbouring spectral lines in the spectrum of acetylene changes as the temperature changes, whereas it remains constant in

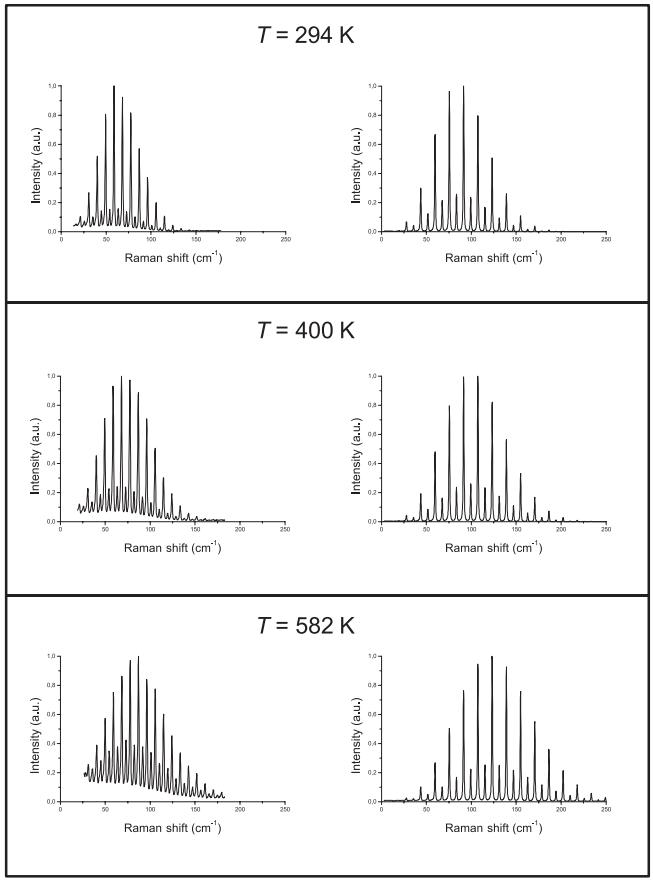

Fig. 1. Experimental rotational CARS spectra of acetylene (*to the left*) recorded at three different temperatures compared with theoretically calculated nitrogen spectra (*to the right*). Note the temperature-dependent intensity alternation in the acetylene spectra

the nitrogen spectra. In order to understand this effect, the vibrational structure of the molecule has to be treated in more detail.

The acetylene molecule has seven fundamental vibrational modes. Of these modes three are non-degenerate, $\nu_1(\Sigma_g^+)$, $\nu_2(\Sigma_g^+)$, and $\nu_3(\Sigma_u^+)$, whereas the remaining four occur as degenegrate pairs, $\nu_4(\Pi_g)$ and $\nu_5(\Pi_u)$. The modes, ν_1, ν_2, and ν_4, are (vibrational) Raman active, and ν_3 and ν_5 are infrared active. The vibrational energy levels are given by

$$G_{[\nu]} = \sum_i \omega_i \left(\nu_i + \frac{d_i}{2}\right) + \sum_i \sum_{k\geq i} x_{ik} \times \left(\nu_i + \frac{d_i}{2}\right)\left(\nu_k + \frac{d_k}{2}\right) + \sum_i \sum_{k\geq i} g_{ik} l_i l_k \,, \quad (1)$$

where ω_i is the vibrational frequency of vibrational mode i, ν_i, and ν_k are vibrational quantum numbers, d_i and d_k are degree of degeneracy for mode i and k ($d_i = 1$ for non-degenerate vibrations, and $d_i = 2$ for doubly degenerate vibrations), x_{ik} and g_{ik} are anharmonicity constants due to coupling between mode i and k, l_i and l_k are vibrational angular momentum quantum numbers which assume the values $l_i = \nu_i, \nu_i - 2, \nu_i - 4, \ldots..$, 1 or 0, and $[\nu]$ stands for all vibrational quantum numbers. For non-degenerate vibrations l_i and g_{ik} are 0. Molecular constants are listed in Table 1, and using these data a vibrational energy level diagram, as illustrated in Fig. 2, can be calculated. As can be seen in this figure, the vibrational structure for acetylene is significantly more complicated than for diatomic molecules. The relative population of a vibrational mode is given by

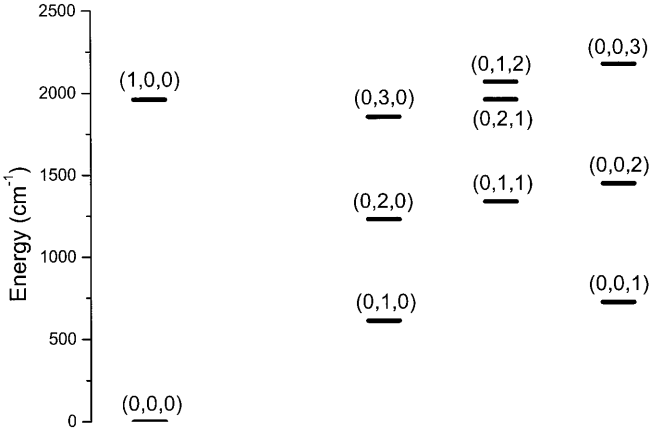

Fig. 2. Vibrational energy level diagram for acetylene calculated using (1) and data from Table 1. The numbers in brackets are vibrational quantum numbers of the vibrational modes ν_2, ν_4, and ν_5, i.e (ν_2, ν_4, ν_5)

$$P(\nu_i) = d_i \exp[-hc\omega_i \nu_i / kT] \,. \quad (2)$$

Since this work is focused on the low-temperature regime it is assumed that the vibrational modes ν_1 and ν_3 are not excited. Figure 3 shows the relative populations of the states $(\nu_2, \nu_4, \nu_5) = (0, 0, 0)$ (the ground state), $(0, 1, 0)$, $(0, 2, 0)$, $(0, 0, 1)$, $(0, 0, 2)$, and $(1, 0, 0)$ as a function of temperature.

Table 1. Values of the molecular constants of acetylene used in the calculation of the rotational CARS spectra

Quantity	Notation	Value	Units	Ref.
Frequencies of the fundamental vibrational modes	ω_i ($i = 1, 2, 3, 4, 5$)	$\omega_1 = 3372.838$ $\omega_2 = 1974.316037$ $\omega_3 = 3294.842$ $\omega_4 = 609.015766$ $\omega_5 = 729.1716034$	cm^{-1}	[31] [32] [31] [32] [32]
Vibrational degeneracy	d_i ($i = 1, 2, 3, 4, 5$)	$d_1 = 1$ $d_2 = 1$ $d_3 = 1$ $d_4 = 2$ $d_5 = 2$		[33]
Coupling constants between vibrational modes	x_{ik} ($i = 2, 4, 5$) ($k = 2, 4, 5$)	$x_{22} = -7.87$ $x_{24} = -12.46$ $x_{25} = -1.52$ $x_{44} = 3.058842$ $x_{45} = -2.433314$ $x_{55} = -2.3357345$	cm^{-1}	[34] [35] [35] [32] [32] [32]
Coupling constants between degenerate vibrational modes	g_{ik} ($i = 4, 5$) ($k = 4, 5$)	$g_{44} = 0.781776$ $g_{45} = 6.582333$ $g_{55} = 3.4899715$	cm^{-1}	[32] [32] [32]
Rotational constant	B_e	1.18229	cm^{-1}	[31]
Vibration-rotational constants	α_i ($i = 1, 2, 3, 4, 5$)	$\alpha_1 = 0.006839$ $\alpha_2 = 0.006187$ $\alpha_3 = 0.00560$ $\alpha_4 = -0.001273$ $\alpha_5 = -0.00235$	cm^{-1}	[31] [31] [31] [31] [31]
Centrifugal distortion constant	D_0	1.6265×10^{-6}	cm^{-1}	[32]
Non-resonant susceptibility	x_{nr}	4.80×10^{-17}	$cm^{-3}erg^{-1}$	[36]
Polarizability anisotropy	ζ_e	1.91×10^{-24}	cm^3	[37]
First derivative	ζ_e'	0	cm^2	
Second derivative	ζ_e''	0	cm	
Nuclear spin statistical weights	g_I	1 sym. levels 3 anti-sym. levels		[38]

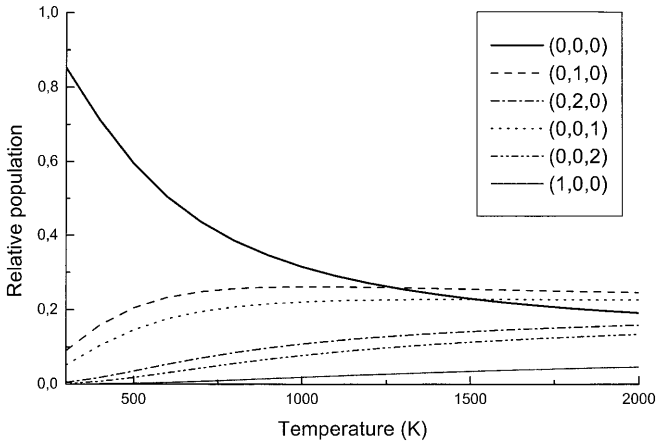

Fig. 3. Relative population (normalized) of the lowest vibrational states of acetylene calculated using (2). Already at room temperature excited states are populated

As the vibrational frequencies of the two doubly degenerate vibrational modes are comparatively low, the relative populations in these excited states are about 15% already at room temperature.

The term values, $F(J)$, of the rotational energy levels for the vibrational ground state and the non-degenerate vibrational modes can be calculated in the same way as for a diatomic molecule:

$$F_{[\nu]}(J) = B_{[\nu]} J(J+1) - D_{[\nu]} J^2 (J+1)^2 \,. \tag{3}$$

In the $B_{[\nu]}$ constant, however, influence from all vibrational modes has to be taken into account. Thus the expressions for $B_{[\nu]}$ is:

$$B_{[\nu]} = B_e - \sum_i \alpha_i \left(\nu_i + \frac{d_i}{2}\right) \,. \tag{4}$$

Since the centrifugal distortion constant, $D_{[\nu]}$, itself is a very small correction term, its dependence on $[\nu]$ is here neglected, i.e. $D_{[\nu]} = D_0$. If also rotational levels within degenerate vibrational states are considered there is a vibrational angular momentum about the internuclear axis, and thus (3) has to be modified:

$$F_{[\nu]}(J) = B_{[\nu]} \left\{ J(J+1) - l^2 \right\} - D_{[\nu]} \left\{ J(J+1) - l^2 \right\}^2 \,. \tag{5}$$

This expression is by analogy with the symmetric-top energy formula of a diatomic molecule, but here with a vibrational angular momentum quantum number l instead of an electronic angular momentum quantum number. For degenerate vibrational levels the rotational quantum number, J, must be larger or equal to l, i.e. levels $J = 0, ..., l-1$ do not occur:

$$J = l, l+1, l+2, ... \,. \tag{6}$$

Thus, each vibrational state consists of a set of rotational levels, however, with slightly different separations (i.e. slightly different rotational constants, B) in the different vibrational levels, and for degenerate levels with the first l rotational levels missing. The differences in energy separations between S-branch rotational lines within different vibrational modes are, however, too small (the shifts for the $J = 10 \rightarrow 12$ transitions in the ground state and the lowest excited state is for example $\approx 0.06\,\mathrm{cm}^{-1}$) to be resolved in multiplex rotational CARS spectra recorded with our equipment. Thus the rotational lines associated to different vibrational bands are overlapping. The total molecular energy $E([\nu], J)$ is of course given by the sum of the vibrational (1) and rotational energy (5):

$$E([\nu], J) = G_{[\nu]} + F_{[\nu]}(J) \,. \tag{7}$$

The rotational levels of a linear molecule are either positive or negative depending on if the total wavefunction remains unchanged or changes sign upon reflection in the origin. In the vibrational ground state, Σ_g^+, the even rotational levels are positive while the odd levels are negative (given that the electronic ground state also is symmetric). In the degenerate vibrational states, i.e. the Π-states, each rotational level consists of two sub-levels, one positive and one negative, of slightly different energies.

For vibrational levels that are symmetric with respect to inversion, all positive rotational levels are symmetric with respect to a simultaneous exchange of all pairs of identical nuclei, whereas the negative ones are antisymmetric (gerade). The opposite holds for vibrational levels that are antisymmetric with respect to inversion (ungerade). In Fig. 4 rotational energy level diagrams with symmetry properties indicated are illustrated for both a non-degenerate and a degenerate vibrational state.

The nuclear spin statistical weight, g_I, of a rotational level is given by the total number of possible orientations of the nuclear spins. In the case of acetylene the spins of the nuclei are 0 for carbon and $1/2$ for hydrogen. Since the nuclear spins of the carbon atoms are zero, only the result of an exchange of the two hydrogen nuclei (identical nuclei) have to be considered. Thus, the statistical weights for the rotational levels of C_2H_2 are the same as for H_2, that is 1 for symmetric levels and 3 for antisymmetric levels. Therefore, a rotational CARS spectrum corresponding to transitions within the non-degenerate vibrational ground state shows an intensity alternation between the rotational lines of 1:9. For the doubly degenerate vibrational states, each rotational state consists of

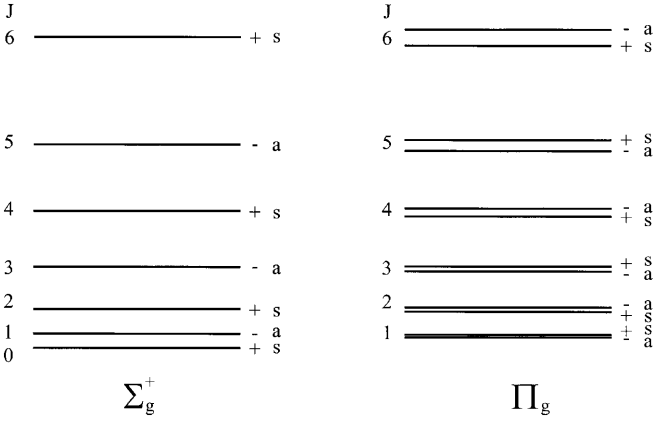

Fig. 4. Rotational energy level diagram of a non-degenerate (Σ_g^+) and a doubly degenerate vibrational state (Π_g) with symmetry properties indicated. For the doubly degenerate vibrational state, each rotational state consists of a symmetric and an anti-symmetric level with a very small energy separation (which is strongly magnified in this figure)

a symmetric and an anti-symmetric level of slightly different energies ($\approx 0.5\,\mathrm{cm}^{-1}$ for $J = 10$), which is not resolvable with our equipment and has therefore been neglected, meaning that the rotational levels are considered as doubly degenerated. The effective statistical weights of these doublets are thus 4, i.e. all levels have the same statistical weights. The rotational lines associated with the two degenerated vibrational states do therefore not show any intensity alternation.

Since the molecular population distribution over different vibrational states is temperature dependent (see Fig. 3), the intensity alternation of the rotational peaks is temperature dependent as well, with a decreasing ratio for increasing temperature, as apparently shown in Fig. 1.

2 Experimental arrangement and measurements

The experimental set-up used was a standard arrangement for dual-broadband rotational CARS experiments similar to that described in [16, 24]. Briefly, the CARS signal was generated by three beams; a narrowband beam of wavelength 532.0 nm and spectral width $\approx 0.7\,\mathrm{cm}^{-1}$ full width at half maximum (FWHM) provided by a Nd:YAG laser, and two broadband beams generated by a dye laser using DCM as dye, arranged in a planar BOXCARS configuration [39]. Using an $f = 1.0$ m spectrograph with a grating of 600 grooves/mm tuned to the fourth order and an intensified diode-array detector (1024 pixels), a spectral dispersion of $0.25\,\mathrm{cm}^{-1}$/pixel was obtained.

The acetylene gas was introduced into a high-pressure cell positioned inside a tube oven (Entech AB, Ängelholm, Sweden). The cylindrical cell had a length of 250 mm and an inside diameter of 12 mm. The cell was equipped with two windows of fused silica, and three thermocouples (type K) positioned along the axial direction over a distance of ≈ 50 mm at the centre of the cell. The temperature measured was very stable in the axial direction, with a difference of less than 0.7% between the different thermocouple readings. Temperature measurements in pure acetylene were performed at atmospheric pressure at six different temperatures: 294, 348, 400, 453, 511, and 582 K. For each temperature, three averaged spectra each consisting of 300 accumulated single-shot spectra were recorded.

Measurements were also carried out in seven different mixtures of acetylene and nitrogen (6.2%, 11.8%, 16.7%, 21.0%, 25.0%, 28.5%, 31.7% acetylene) at room temperature and atmospheric pressure. Since these measurements were performed at room temperature, the gas mixtures were introduced into the CARS probe volume as a stable flow inside a pipe. Thus, the cell and oven could be removed, and thereby spectral contributions from stray light (originating from the Nd:YAG laser) due to multiple reflections in the optical windows of the cell were avoided. Acetylene and nitrogen of high purity were mixed and passed through the pipe. The different mixtures were adjusted using two mass flow controllers. For each mixture, three averaged spectra, each consisting of 300 accumulated single-shot spectra, were recorded.

For each measurement, a background spectrum, consisting of 300 accumulated single-shot spectra, was recorded with the dye laser beam superimposed on the Nd:YAG laser beam blocked. In connection with each measurement series several accumulated (300 shots) non-resonant CARS spectra were recorded in argon gas at ambient conditions. By taking intensity ratios at each pixel between the recorded spectra and an argon spectrum, the spectra were compensated for the differences in probability of generating anti-Stokes photons at different frequencies, and for the differences in sensitivity of the detector pixels. The non-linear response of the diode-array detector to the intensity of the CARS signal was compensated for in the subsequent evaluation of the recorded spectra [40].

3 Spectral evaluation

3.1 Spectral calculation

The computer code for simulating rotational CARS spectra used in the present work originates from a vibrational CARS code developed by Hall and others [41–44]. This code was modified by Kröll [40], and from this a code for rotational CARS was written by Nilsson [45, 46]. Substantial development was then carried out by Martinsson et al. [13, 24].

Calculation of a rotational CARS spectrum can be divided into two parts: calculation of the third-order susceptibility, $x^{(3)}_{\mathrm{CARS}}$, and convoluting the squared modulus of $x^{(3)}_{\mathrm{CARS}}$ by the laser line intensity profiles and the slit function. The rotational CARS susceptibility for n different species can be written:

$$x^{(3)}_{\mathrm{CARS}} = x_{\mathrm{nr}} + \sum_n \sum_{J_n} \frac{a_{J_n J'_n}}{\omega_{J_n J'_n} - \omega_1 + \omega_2 - \mathrm{i}p\Gamma_{J_n J'_n}/2}\,, \qquad (8)$$

where x_{nr} is the non-resonant susceptibility of the mixture i.e. the mole fraction average of the non-resonant susceptibilities of the n different species, $\omega_{J_n J'_n} = \left\{E\left([\nu]_n\,,\,J'_n\right) - E\left([\nu]_n\,,\,J_n\right)\right\}/\hbar$ is the transition frequency between the rotational levels J_n and J'_n, ω_1 and ω_2 are for dual-broadband rotational CARS the frequencies of the two dye laser photons that drive the rotational Raman resonances, p is the pressure, $\Gamma_{J_n J'_n}$ is the rotational Raman line-broadening coefficient at FWHM, and $a_{JJ'}$ is the rotational line strength which is expressed as:

$$a_{J_n J'_n} = \frac{4}{45}\frac{N_n}{\hbar}\zeta^2_{n,\nu} b^{J'_n}_{J_n} \Delta\varrho_{J_n J'_n} F_n\left(J_n\right)\,, \qquad (9)$$

where N_n is the number density of species n, $\zeta_{n,\nu}$ is the polarizability anisotropy change due to vibrational anharmonicity [47, 48], $b^{J'_n}_{J_n}$ is the Placzek–Teller coefficient [49], $\Delta\varrho_{J_n J'_n}$ is the normalized population difference between the rotational levels J_n and J'_n, and $F_n\left(J_n\right)$ is a correction factor due to centrifugal distortion [50, 51]. In order to include the relative population of the different vibrational modes of acetylene the expression for the number density is expressed:

$$N_n = x_n P_n\left(\nu_i\right)\,, \qquad (10)$$

where x_n is mole fraction of species n and $P_n\left(\nu_i\right)$ is the relative population in different vibrational modes. Denoting nitrogen species 1 and acetylene species 2 for nitrogen/acetylene mixtures $P_1(\nu) = 1$ (since nitrogen has only one vibrational mode) and $P_2(\nu_i)$ is given by (2). The normalized pop-

ulation difference can be expressed as:

$$\Delta\varrho_{J_n J_n'} = \frac{g_{I_n}\,(2J_n+1)}{Q_{J_n}} \left\{ \exp\left[-\frac{E\,([\nu]_n\,,\,J_n)}{kT} \right] - \exp\left[-\frac{E\,([\nu]_n\,,\,J_n')}{kT} \right] \right\}\,, \tag{11}$$

where g_{I_n} is the statistical weight factor due to the nuclear spin degeneracy, Q_{J_n} is the rotational partition function, and $E\,([\nu]_n,\,J_n)$ is the energy in vibrational state $[\nu]_n$ and rotational state J_n of the molecule.

The effects of the laser linewidths and the instrumental function (slit function) must also be considered. For broadband CARS, the influence due to laser intensity profiles is taken into account by convoluting the squared modulus of the susceptibility expression (8) with the laser line intensity profiles. Since the pump laser used in the present study was multi-mode (linewidth 0.7 cm^{-1}, FWHM), and as the beams were uncorrelated, the convolution was performed according to the Kataoka–Teets expression [52, 53]:

$$\begin{aligned} I_{\mathrm{KT}}\,(\omega_{\mathrm{KT}}) = & K \iiint \left| \frac{1}{2} x^{(3)}_{\mathrm{CARS}}\,(\omega_1-\omega_2) \right. \\ & \left. + \frac{1}{2} x^{(3)}_{\mathrm{CARS}}\,(\omega_3-\omega_2) \right|^2 \\ & \times I_1\,(\omega_1)\,I_2\,(\omega_2)\,I_3\,(\omega_3) \\ & \times \delta\,(\omega_1-\omega_2+\omega_3-\omega_{\mathrm{KT}})\,\mathrm{d}\omega_1\mathrm{d}\omega_2\mathrm{d}\omega_3\,, \end{aligned} \tag{12}$$

where K is a scalar constant, $I_1\,(\omega_1)$, $I_2\,(\omega_2)$, $I_3\,(\omega_3)$ are the irradiances associated to each laser beam involved, and δ is the Dirac delta function. Analytical expressions for the Kataoka–Teets convolution can be found in for example [1, 54, 55]. Finally the influence of the detection system on the recorded CARS spectra is taken into account by convoluting the CARS intensity with an instrumental function, which in our case is performed using an FFT algorithm [56].

3.2 Approximations made for acetylene

Due to the comparatively high complexity of the molecular structure of acetylene, several approximations have been made, and below the most important ones are listed.

- Since the measurements were performed at relatively low temperatures the vibrational modes ν_1 and ν_3 are assumed to be unpopulated, and their contributions to the rotational CARS spectra have therefore been neglected. This approximation is supported by the result presented in Fig. 3.
- For the two doubly degenerated vibrational modes, each rotational state consists of two levels of slightly different energies, corresponding to the two directions of the angular momentum l. The energy splitting $\Delta\nu$, however, increases with increasing rotation, i.e. with increasing value of J, following the relation: $\Delta\nu = qJ\,(J+1)$, where q is the l-type doubling constant. The values of the l-type doubling constants for the two degenerated vabrational states are $\approx 5\times10^{-3}\,\mathrm{cm}^{-1}$ for both states, which implies an energy separation of $\approx 0.5\,\mathrm{cm}^{-1}$ for $J=10$, which is not resolvable with our detection system. However, a detailed comparison of the spectra recorded at 294 K and 582 K shows that the rotational peaks at 582 K are somewhat broader than at 294 K. Moreover, the spectral positions of the peaks are slightly shifted with temperature. These observations indicate the effect of l-type doubling since overlapping contributions from rotational peaks generated within the non-degenerated ground state and the two components generated in doubly degenerated vibrational states result in broadening and spectrally shifted peaks. The spectral shifting can be explained by the different statistical weights of the two l-components within the degenerated vibrational states. Since our measurements are performed at low temperatures, i.e. when only low rotational states are populated (i.e. the values of J are low) the energy splitting due to l-type doubling has been omitted in the spectral calculation. This means that the rotational level splitting indicated for the Π_g-state in Fig. 4 is in our calculation replaced by doubly degenerated levels.
- A particularly important factor is the polarizability anisotropy since the rotational line strength scales quadratically to this term (as given by (9)). The polarizability anisotropy in vibrational state v can be expressed as [47, 48]:

$$\zeta_v = \zeta_e + \zeta_e'\langle r-r_e\rangle_v + 0.5\zeta_e''\langle r-r_e\rangle_v^2 + \ldots..\,, \tag{13}$$

where ζ_e' and ζ_e are the first and second order derivative of the polarizability anisotropy with respect to the internuclear distance r at the equilibrium distance r_e, and $\langle r-r_e\rangle_v$ is the average deviation from the internuclear distance in vibrational level v. Since no values of ζ_e' and ζ_e'' have been found in the literature, the influence of the increasing internuclear distance for higher vibrational states on the polarizability anisotropy has not been taken into account. Hence, the polarizability anisotropy has the same value for all vibrational levels within a particular vibrational mode. These values are given in Table 1. Moreover, the value of the polarizability anisotropy is expected to be slightly different for different vibrational modes [57]. However, since the difference between the vibrational ground state (0,0,0) and the highest mode here considered (1,0,0) is less than 1.5%, all vibrational states have been assumed to have the same value.
- The correction to the rotational line strengths due to centrifugal distortion may be expressed as [50, 51]:

$$F\left(J,\,J'\right) = 1+\frac{8}{\eta}\left(\frac{B_e}{\omega_e}\right)^2\left(J^2+3J+3\right)$$
$$\text{where} \qquad \eta = \frac{\zeta_e}{r_e\zeta_e'}\,. \tag{14}$$

Since no value on ζ_e' has been found, no correction due to centrifugal distortion has been made, and the value of $F\left(J,\,J'\right)$ is in the present case equal to one. This term has its strongest influence for high temperatures, i.e. when high rotational quantum numbers J significantly contribute to the spectra. Therefore, the current approximation will not imply any significant errors in the evaluation of the spectra measured under the present conditions.
- Since the vibrational ground state is totally symmetric (Σ_g^+) the rotational Raman selection rule is $\Delta J = \pm 2$.

Thus, the ground state pure rotational CARS spectrum consists of an S-branch ($\Delta J = +2$) only. For the doubly-degenerated vibrational modes, however, each J-transition is a doublet, which means that also Raman transitions with $\Delta J = \pm 1$ are allowed, meaning that also an R-branch ($\Delta J = +1$) will appear in the rotational CARS spectrum. However, no contributions due to R-branch transitions are visible in the recorded spectra. Since the intensity of R-branch transitions scale as J^{-1}, these transitions disappear very quickly for increasing J. Therefore, the R-branch transitions have been neglected in the calculation of rotational CARS spectra.

3.3 Raman linewidth considerations

Accurate values for the rotational Raman linewidths of acetylene are of great importance for calculation of theoretical rotational CARS spectra, both regarding the evaluation of temperature and concentration. To our knowledge, no values for pure rotational S-branch Raman transitions have been reported. However, a great number of papers report on measurements of both self-broadened [58–62] and nitrogen-broadened linewidths [63–67] by infared absorption spectroscopy. Self-broadened Raman linewidths of acetylene have been measured by high-resolved continuous wave (cw) CARS for the Q-branch of the ν_2-band at room temperature [68, 69]. The linewidths measured by Fabelinsky et al. [68] are expressed as $\Gamma = ap + b$, where $a = 0.21\,\mathrm{cm^{-1}atm^{-1}}$ is the pressure-broadening contribution, p is the total pressure, and $b = 0.01\,\mathrm{cm^{-1}}$ is the Doppler-broadening term. However, no dependence on the rotational quantum number, J, is reported in these papers.

In the present evaluations the linewidth measured by Fabilinsky et al. [68] is used. However, as no J-dependence is reported, we have also combined these linewidths with the J-dependence calculated for nitrogen using a semi-classical approach [70]. Thus, the expressions for the linewidths (FWHM) using the two models are given by:

$$\Gamma(T) = 0.22\sqrt{\frac{300}{T}} \quad (\mathrm{cm^{-1}}) \qquad \text{(Model A)}\,,$$

$$\Gamma(T, J) = 0.22\sqrt{\frac{300}{T}} + \Gamma(T, J)_{\mathrm{N_2}} - \Gamma(T, 0)_{\mathrm{N_2}} \quad (\mathrm{cm^{-1}}) \qquad \text{(Model B)}\,.$$

As can be seen in these expressions, it is assumed that the linewidths scale as $T^{-0,5}$. This assumption is the same as was used by Farrow et al. [4] and Lucht et al. [5] for calculation of vibrational CARS spectra. Moreover, since no measurements or calculations of acetylene Raman linewidths perturbed by nitrogen have been published, no influence of perturbing nitrogen molecules on the Raman linewidths is included in the present models. Both approximations certainly imply errors in the temperature and concentration evaluations. However, the first assumption is probably most critical since it has been shown, for rotational CARS spectra of nitrogen, that the J-dependence of the rotational Raman linewidths, rather than their magnitude, is most important for the evaluated temperature [13]. The two linewidth models are displayed in Fig. 5.

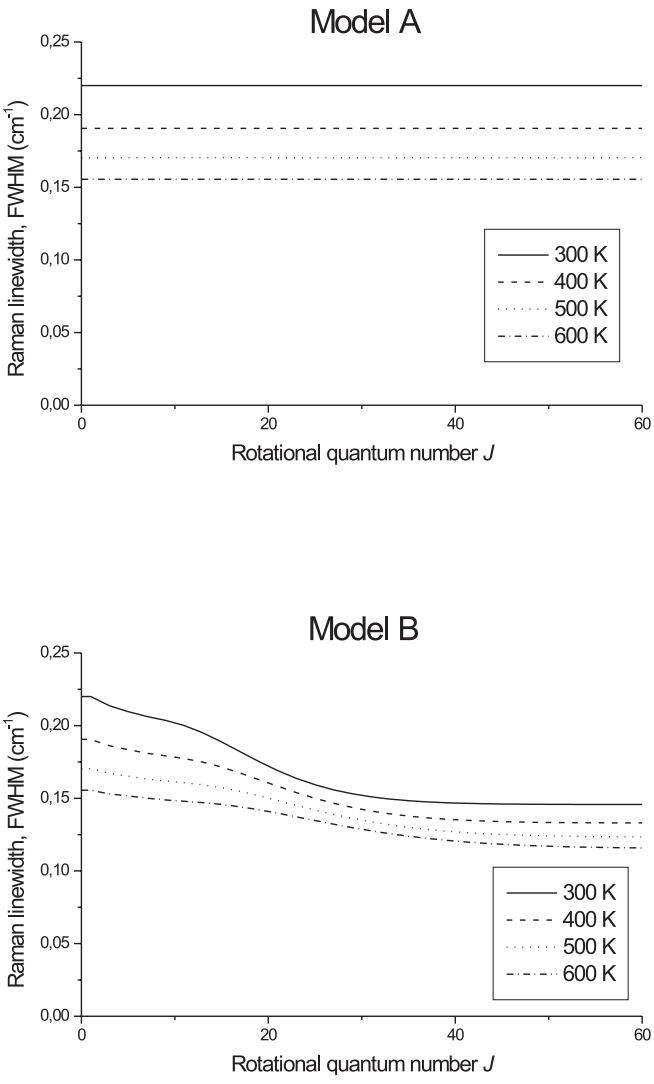

Fig. 5. Plots of the two different Raman linewidth models used for acetylene. Both models are based on the value reported by Fabelinsky et al. [68]. For model B, however, a J-dependence calculated for nitrogen [70] is added to the linewidth measured by Fabelinsky et al.

3.4 Evaluation routine

Both temperature and relative acetylene-to-nitrogen concentration are evaluated by a least-square fitting of libraries of theoretically calculated spectra to the experimental spectrum. Each library contains simulated spectra in the temperature range 300–600 K with a grid of 100 K. Generally, four parameters; the temperature, the linear dispersion, the Raman shift corresponding to a specific detector pixel, and the non-resonant susceptibility were varied using a Marquardt algorithm [71] until a global minimum of the sum-of-squares difference (SSQ) between the experimental and the theoretical spectrum is found. Figure 6 shows evaluated spectra for three different temperatures using model B for the Raman linewidths. In addition to the experimental spectra the difference between the experimental and the best-fitted calculated spectra are indicated by the lower difference-curves in this figure. It is clear that the quality of the spectral fit is best at the lowest temperature. For the two higher temperatures the quality becomes worse due to larger mismatches at spec-

tral positions corresponding to the resonant transitions. These mismatches give rise to spectral features in the difference-curves that indicate that the experimental peaks are broader than the calculated ones, and that the spectral positions of the experimental peaks are slightly different in comparison with the calculated peaks. A possible explanation for this is the neglecting of the energy splitting of the rotational levels due to *l*-type doubling in the degenerated vibrational states. At 582 K about half the number of molecules populate degenerate vibrational states, and the rotational CARS signal generated by these molecules will contribute equally as much to the shape of the rotational CARS spectrum as the molecules in the ground state. Since each rotational level within the doubly-degenerated vibrational states is split into two components of slightly different energies ($\approx 0.5\,\mathrm{cm}^{-1}$ for $J = 10$) due to *l*-type doubling, a broadening approximately proportional to J^2 of the rotational peaks is expected. Moreover, since the strength of the resonant rotational peaks of the two components is different due to different statistical weights, the rotational peaks associated with the doubly-degenerated vibrational states might be spectrally shifted in comparison with the calculated peaks, for which the rotational levels are considered degenerated.

When simultaneously relative acetylene concentration is to be evaluated, libraries corresponding to different acetylene mole fractions covering a range of concentrations around the expected concentration with a grid of 0.5% are used. For each concentration in the library a temperature is evaluated and a value of the SSQ is obtained. This procedure is repeated for all acetylene concentrations. The concentration is determined from the minimum SSQ found by fitting of a third-order polynomial to the SSQs as a function of acetylene fraction. The corresponding temperature is then evaluated by interpolating between the temperatures evaluated for the different acetylene mole fractions. Figure 7 shows evaluated spectra

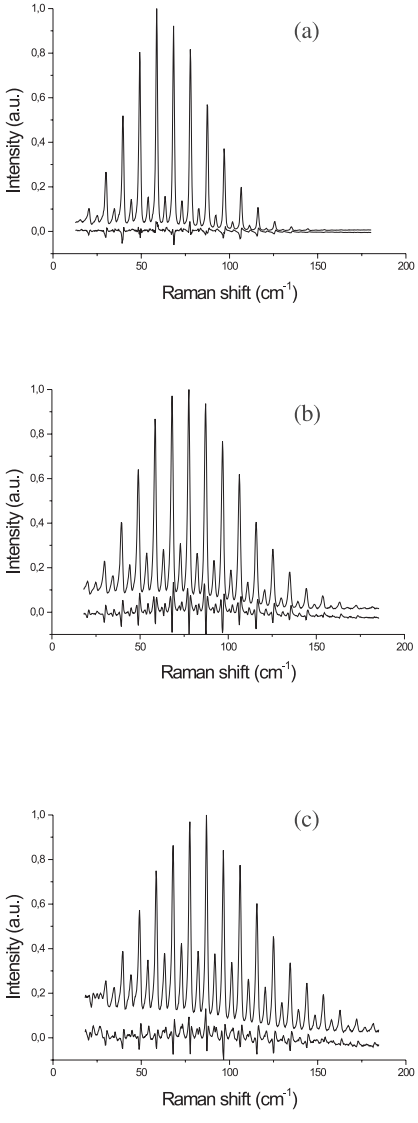

Fig. 6a–c. Evaluated rotational CARS spectra recorded in pure acetylene at three different temperatures; 294 K (**a**), 453 K (**b**), and 582 K (**c**), using Raman linewidth model B. The *lower curves* are differences between the experimental spectra and the best-fitted theoretical spectra

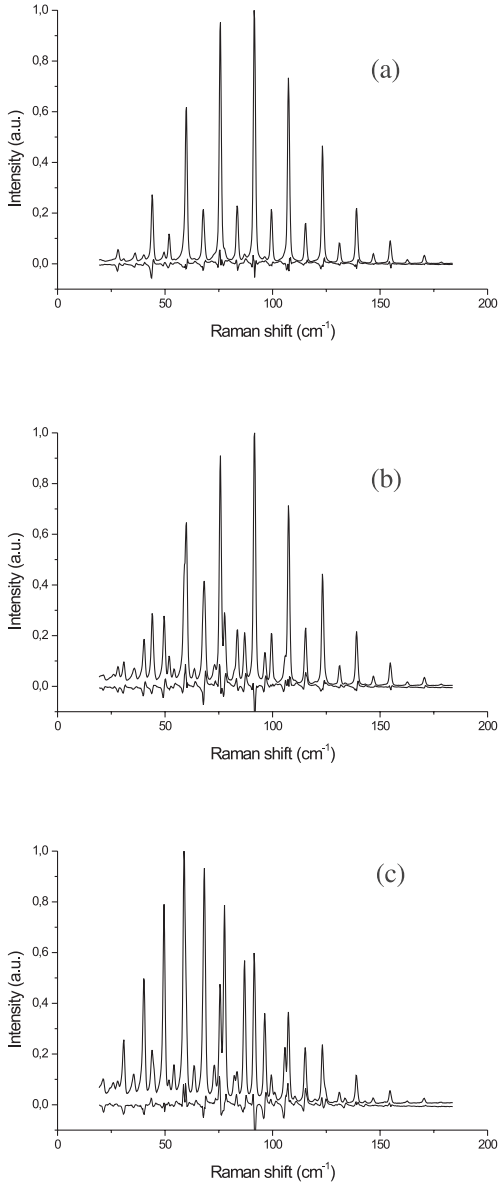

Fig. 7a–c. Evaluated rotational CARS spectra recorded in different mixtures of acetylene and nitrogen; **a** 6.2%, **b** 16.7%, and **c** 31.7% acetylene

for three different acetylene mole fractions using model B for the rotational Raman linewidths. This figure clearly illustrates that the shape of the rotational CARS spectra drastically changes with the acetylene mole fraction. Since the polarization anisotropy of acetylene [37] is ≈ 2.8 times higher than for nitrogen [48], the shape of the spectrum recorded in the mixture consisting of 31.7% acetylene (see Fig. 7c) is dominated by the acetylene lines.

4 Results

Before evaluating the spectra recorded in pure acetylene and different acetylene/nitrogen mixtures, three averaged spectra each consisting of 300 accumulated spectra recorded in ambient air were evaluated in order to determine the slit function of the detection system. These spectra were evaluated with the value of the non-resonant susceptibility fixed to the theoretical value of air and using several theoretical libraries consisting of spectra convoluted with Lorentzian slit functions of different half-widths. From these evaluations it was found that a slit width of $0.5\,\mathrm{cm}^{-1}$ (FWHM) gave the best spectral fit, i.e. the lowest SSQ. Thus all theoretical spectra used in the evaluations were convoluted with a $0.5\,\mathrm{cm}^{-1}$ (FWHM) Lorentzian slit function.

4.1 Temperature measurements in pure acetylene

The results of the measurements performed in pure acetylene with the non-resonant susceptibility fitted are presented in Table 2 and the temperatures are illustrated in Fig. 8. The evaluated temperatures are mean values of three averaged spectra, each consisting of 300 recorded single-shot spectra. The evaluation has been performed using two sets of Raman linewidths, model A and model B as described above. The results obtained for model A indicate an almost constant overprediction of around 25 K for the entire temperature regime. The temperatures evaluated using model B are, however, in good agreement with the temperatures measured by thermocouples, in general with a relative error of less than 2%. The differences between the lowest and highest temperatures evaluated from the three averaged spectra at each temperature are generally smaller than 1% except for the measurements performed at 348 K where it is $\approx 3\%$. This measurement point also shows the greatest temperature error for both linewidth models used. Both the temperature error and the quality of the spectral fit for the first two spectra recorded at this condition is significantly worse than for the last spectra, which might indicate any spectral interference in the first two spectra. However, this effect was not visible by eye during the recordings.

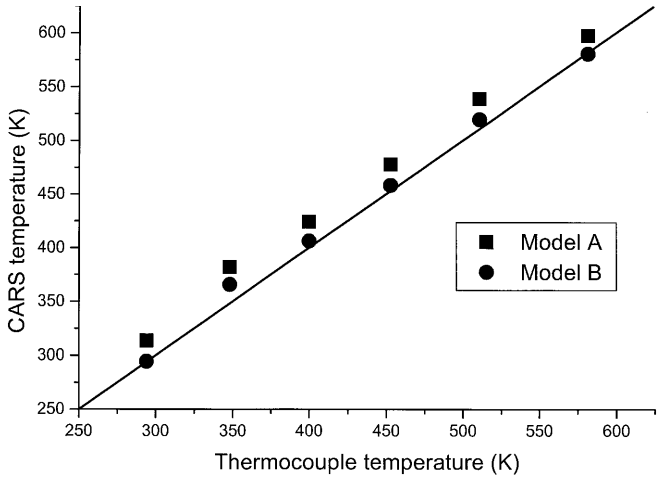

Fig. 8. Resulting mean temperature of three spectra consisting of 300 accumulated single-shots recorded in pure acetylene vs. thermocouple temperature. The temperatures were evaluated using the two different Raman linewidth models and by fitting the value of the non-resonant susceptibility. The *straight line* indicates perfect agreement and is only included for comparison purpose

The measured data were also evaluated with the non-resonant susceptibility fixed to the literature value of acetylene ($4.8 \times 10^{-17}\,\mathrm{cm}^{-3}\mathrm{erg}^{-1}$ [36]). The differences between the evaluated temperatures and the thermocouple temperatures obtained with and without fitting the value of the non-resonant susceptibility are compared in Fig. 9. As illustrated in Fig. 9a, the temperature errors obtained using model A, increase roughly linearly with the temperature when the non-resonant susceptibility is fixed. The results obtained using model B, displayed in Fig. 9b, show a different behaviour; the error increases almost linearly for temperatures up to 453 K where a maximum is reached. For the two highest temperatures the temperature error decreases with increasing temperature to ≈ 30 K at 582 K. Thus, spectral evaluation without fitting the value of the non-resonant susceptibility implies large temperature errors for both linewidth models used. By fitting the value of the non-resonant susceptibility these errors are significantly reduced for both linewidth models, however, the highest accuracy is obtained by using linewidth model B.

The evaluated values of the non-resonant susceptibility are displayed in Fig. 10. As illustrated in this diagram, the fitted values are ≈ 2–2.5 times the literature value for acetylene ($4.8 \times 10^{-17}\,\mathrm{cm}^{-3}\mathrm{erg}^{-1}$ [36]. In addition, the theoret-

Table 2. Resulting data from temperature measurements in pure acetylene using the following designations: T_{th} = temperature measured by the thermocouples, $\langle T\rangle$ = mean temperature measured by rotational CARS, and $\langle \chi_{\mathrm{nr}}\rangle$ = evaluated mean value of the non-resonant susceptibility when it is fitted in the evaluation of the spectra

T_{th} /K	$\langle T\rangle$ /K		$(\langle T\rangle - T_{\mathrm{th}})/T_{\mathrm{th}}$ /%		$\langle x_{\mathrm{nr}}\rangle /10^{-17}$ $\mathrm{cm}^{-3}\mathrm{erg}^{-1}$	
	Model A	Model B	Model A	Model B	Model A	Model B
294	314	297	6.8	1.0	9.3	10.9
348	382	368	9.8	5.7	9.2	10.4
400	424	408	6.0	2.0	10.1	11.2
453	478	459	5.5	1.3	10.9	12.0
511	539	520	5.5	1.8	10.0	11.1
582	598	582	2.7	0	10.4	11.9

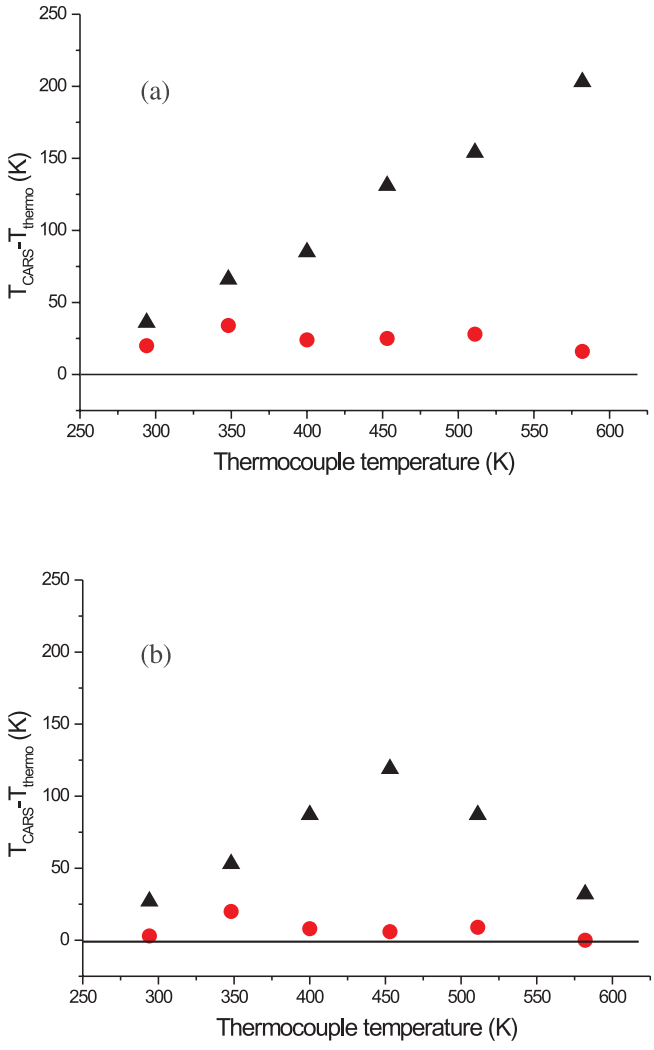

Fig. 9a,b. Difference between the evaluated mean temperature of three spectra consisting of 300 accumulated single-shots and the thermocouple temperature vs. thermocouple temperature for pure acetylene using linewidth model A (**a**) and B (**b**), respectively. The data points designated by *triangles* correspond to evaluations with the non-resonant susceptibility fixed at the literature value of acetylene, whereas the *circles* correspond to results obtained when the non-resonant susceptibility is fitted in the evaluation routine

ical libraries calculated using linewidth model B result in 10%–15% higher values of the non-resonant susceptibility than those found by using model A. The spread in the three

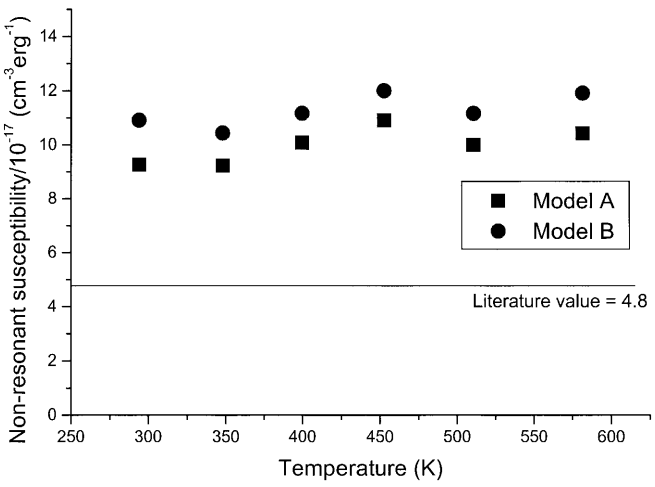

Fig. 10. The fitted value of the non-resonant susceptibility obtained from measurements in pure acetylene as a function of the thermocouple temperature for the two different linewidth sets. The literature value of the non-resonant susceptibility for acetylene (4.8×10^{-17} $cm^{-3}erg^{-1}$) is also displayed

values of the non-resonant susceptibility evaluated for each temperature was small for both linewidth models used; less than 4.5% of the mean value for all temperatures except at 348 K where it was 15%.

4.2 Simultaneous relative acetylene concentration and temperature measurements

The results of the acetylene concentration measurements performed at room temperature and atmospheric pressure are summarized in Table 3 and the evaluated concentrations are illustrated in Fig. 11. The presented results are mean values of three averaged spectra, each consisting of 300 recorded single-shot spectra. The results for the two different linewidth models used are quite similar. The maximum error is, however, slightly greater for model B; 3.6% on an absolute scale corresponding to 12.6% on a relative scale. The simultaneously evaluated temperatures are shown in Fig. 12, and are, as clearly indicated, in good agreement with the ambient temperature for the lowest acetylene concentration but increase with increasing acetylene concentration for both linewidth models used. The difference between the highest and lowest evaluated temperature is, however, larger for model A (21 K) than for model B (9 K).

Table 3. Results from simultaneous acetylene concentration and temperature measurements in different mixtures of acetylene and nitrogen. The designations stands for: x = acetylene mole fraction measured by mass-flow controller, $\langle c \rangle$ = measured mean acetylene concentration, $\Delta c = \langle c \rangle - x$ (i.e. absolute error of the measured concentration), and $\langle T \rangle$ = measured mean temperature

x /%	$\langle c \rangle$ /%		Δc /%		$\Delta c/x$ /%		$\langle T \rangle$ / K	
	Model A	Model B	Model A	Model B	Model A	Model B	Model A	Model B
6.2	6.5	5.7	0.3	−0.5	4.8	8.1	295	295
11.8	12.6	11.7	0.8	−0.1	6.8	0.8	297	298
16.7	17.8	17.1	1.1	0.4	6.6	2.4	302	299
21.0	22.9	22.5	1.9	1.5	9.0	7.1	308	304
25.0	27.2	27.0	2.2	2.0	8.8	8.0	312	306
28.5	31.0	32.1	2.5	3.6	8.8	12.6	313	303
31.7	34.4	34.6	2.7	2.9	8.5	9.1	316	304

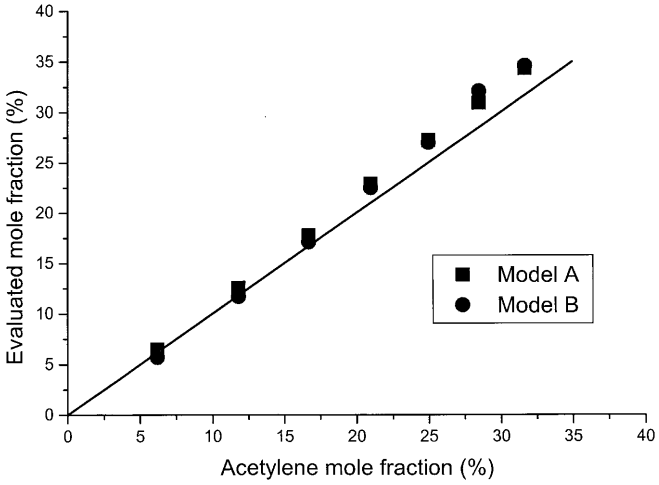

Fig. 11. Evaluated relative acetylene-to-nitrogen concentration; mean value of three spectra consisting of 300 accumulated single-shots vs. concentration set by mass-flow controllers for the two different sets of Raman linewidths. The *straight line* indicates perfect agreement and is only included for comparison purpose

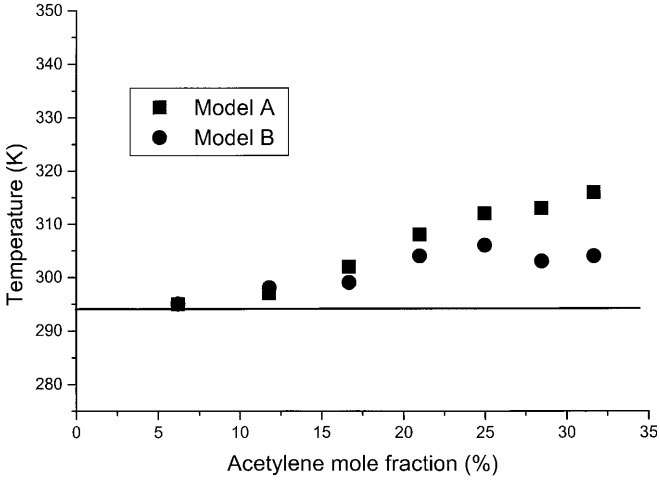

Fig. 12. Evaluated temperature; mean value of three spectra consisting of 300 accumulated single-shots vs. acetylene concentration set by mass-flow controllers for the two different sets of Raman linewidths. The value of the ambient temperature, 294 K, is also displayed

The evaluated non-resonant susceptibilities, relative to the literature value for pure nitrogen ($0.74 \times 10^{-17}\,\mathrm{cm^{-3}erg^{-1}}$ [72]), for the different acetylene concentrations investigated are shown in Fig. 13. Theoretical values of the non-resonant susceptibilities corresponding to the different compositions are calculated as the average of the values for nitrogen and acetylene, weighted in accordance with the present mixtures, and these values are, for comparison, also indicated in Fig. 13. Similar to the results for pure acetylene (see Fig. 10), the evaluated values are higher than the theoretical for both acetylene linewidth models used. For acetylene concentrations up to 21%, the experimental values show a linear dependence on the present acetylene concentration for both linewidth models. For the three highest concentrations, however, the evaluated values show a stronger dependence on the acetylene mole fraction.

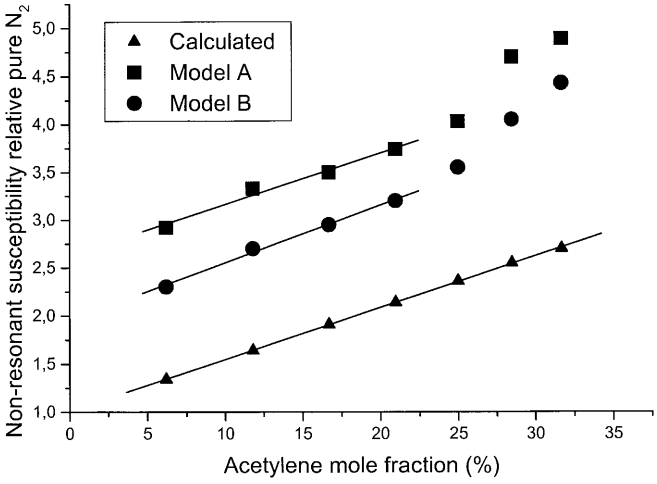

Fig. 13. The fitted value of the non-resonant susceptibility relative the literature value of nitrogen ($0.74 \times 10^{-17}\,\mathrm{cm^{-3}erg^{-1}}$ [72]) obtained from measurements in different acetylene/nitrogen mixtures as a function of acetylene concentration set by mass-flow controllers for the two different sets of Raman linewidths. For the measured data obtained at the four lowest concentrations, linear functions have been fitted. Theoretically calculated non-resonant susceptibilities are also displayed

5 Discussion

5.1 Temperature measurements in pure acetylene

The result presented in Fig. 8 shows that by using the present two assumptions for the J-dependence of the rotational Raman linewidths of acetylene, and by fitting the non-resonant susceptibility, temperatures of reasonable accuracy can be obtained using dual-broadband rotational CARS. The reason for this is most probably, similar to nitrogen [13], due to the strong temperature sensitivity of the spectral shape at low temperatures. The spectral shape is mainly determined by the resonant spectral lines, i.e. the resonant part of the third-order susceptibility, which, using (8), (9), and (10), for pure acetylene at atmospheric pressure can be expressed as (disregarding the laser line convolutions, the convolution with the slit function, and J-dependent factors):

$$\left|x_r\left(\omega\right)\right|^2 \propto \frac{\left[P\left(\nu_i\right)\zeta_\nu^2 \Delta\varrho_{JJ'}\right]^2}{\left(\omega_{JJ'}-\omega\right)^2+\Gamma_{JJ'}^2/4}\,. \tag{15}$$

In this expression there are especially three parameters that change with temperature; the relative population in different vibrational modes $P(\nu_i)$, the population difference factor $\Delta\varrho_{JJ'}$, and the Raman linewidth $\Gamma_{JJ'}$. The values of $P(\nu_i)$ and $\Delta\varrho_{JJ'}$ follow well-known Boltzmann distributions given by (2) and (11), respectively, whereas the values of the S-branch rotational Raman linewidths $\Gamma_{JJ'}$ are based on approximate assumptions (Models A and B). Hence, the Raman linewidth is among these the most uncertain parameter.

Another source of spectral and thereby temperature errors is the J-dependent energy splitting of the two l-components of the rotational levels belonging to degenerate vibrational states. Since the energy splitting is proportional to $J(J+1)$, neglecting the energy splitting leads to increasing spectral errors with temperature. In addition, the population of degenerated vibrational states increases with temperature as shown in Fig. 3. Therefore, temperature errors due to energy splitting

of the rotational levels are expected to increase with increasing temperature, and with a fixed value of the non-resonant susceptibility in the spectral evaluations this is also supported by the result using linewidth model A (see Fig. 9a). The corresponding graph for model B (see Fig. 9b) shows similar results for temperatures up to 453 K, however, for the two highest temperatures the temperature errors are significantly lower and decrease with temperature. A possible explanation for this might be that the *J*-dependent spectral influence of energy splitting of the rotational lines is compensated by *J*-dependent errors in linewidth model B (see Fig. 5).

In contrast to nitrogen, a rotational CARS spectrum of acetylene shows a temperature-dependent intensity alternation between the rotational lines (see Fig. 1) due to excitation of doubly-degenerated vibrational modes. This implies, as previously mentioned, additional temperature information. However, since the vibrational structure of acetylene is comparatively complicated, several approximations were made (see Sect. 3.2), which of course imply errors in the simulated rotational CARS spectra, upon which the temperature is evaluated.

Beside the approximations described in Sect. 3.2, the slit function, i.e. the influence of the detection system on the recorded spectra, and the non-resonant susceptibility are two uncertain parameters in the evaluation of the spectra. The shape of the slit function is difficult to experimentally determine and may also change during measurements [13]. The value of the slit width is, thus, a potential source of errors, regarding both temperature and relative acetylene concentration measurements. The non-resonant susceptibility is in a rotational CARS spectrum mainly manifested by a background level, but it also has an influence on the shape of the rotational lines. The uncertainty of the value of the non-resonant susceptibility of acetylene is at least ±20% [36]. For nitrogen and mixtures of nitrogen and oxygen, it has been shown previously that, by fitting the non-resonant susceptibility in the spectral evaluation, both the quality of the spectral fits and the temperature accuracy are significantly improved [13, 14]. In these papers it is also concluded that fitting the non-resonant susceptibility can compensate small errors (up to 20%) in the slit width. Due to the relatively large uncertainties in the values of the slit width and the non-resonant susceptibility of acetylene, the non-resonant susceptibility has also been fitted in the present study and the results are shown in Figs. 8 and 9. In Figs. 9a and 9b the results are compared to the results obtained without fitting of the non-resonant susceptibility for the two different Raman linewidth models used. As apparently shown in Fig. 9 the temperature accuracy is significantly improved, for both linewidth models used, when the non-resonant susceptibility is fitted. The results also indicate that beside compensating possible errors in the slit width, also temperature errors caused by neglecting the *J*-dependent energy splitting due to *l*-type doubling of the rotational levels associated with the degenerated vibrational states are significantly reduced by fitting the non-resonant susceptibility. It is therefore not surprising that the evaluated values of the non-resonant susceptibilities (see Fig. 10) deviate significantly (about 100%) from the literature value of acetylene.

In comparison with rotational CARS thermometry of nitrogen and oxygen [13, 24] the present results for acetylene show that fitting of the non-resonant susceptibility has a much larger influence on the evaluated temperature, and is, with the present model, apparently necessary in order to achieve a high temperature accuracy. The results also show that using a Raman linewidth model that assumes *J*-dependent linewidths gives a higher temperature accuracy than a model without any *J*-dependence. It is however a very rough assumption to use a *J*-dependence calculated for nitrogen, and further theoretical and experimental work regarding rotational Raman linewidth broadening coefficients for acetylene will probably improve the technique for acetylene thermometry.

5.2 Simultaneous relative acetylene concentration and temperature measurements

The potential for relative acetylene to nitrogen concentration measurements using rotational CARS is interesting to investigate since it possibly provides a tool for local measurements of fuel/air equivalence ratios, especially at the lower temperatures in the mixing and precombustion zones, in combustion processes. A stoichiometric acetylene/air mixture contains an acetylene mole fraction of 0.08. Thus, the conditions investigated in the present study; acetylene/nitrogen mixtures in the range 0.06–0.32 mole fraction acetylene at room temperature, corresponds to typical conditions prevailing in the low-temperature mixing and pre-combustion zones of premixed acetylene/air flames.

The results of the measurements presented in Fig. 11 show good accuracy for the three lowest acetylene mole fractions whereas the accuracy successively deteriorates with increasing concentration for the four highest acetylene concentrations. The result of relative concentration measurements by rotational CARS is strongly dependent on the resonant part of the third-order susceptibility corresponding to the different species, which is given in (15). Thus, uncertainties in the relative population of different vibrational modes $P(\nu_i)$, the polarizability anisotropy ζ_ν, the population difference factor $\Delta\varrho_{JJ'}$, and the Raman linewidth $\Gamma_{JJ'}$ will influence the evaluated acetylene concentration.

The value of the polarizability anisotropy is especially critical since the rotational linestrength scales quadratically to the value of this parameter. The uncertainty in the value of the polarizability anisotropy found in the literature is $\approx 2\%$ [37], and since no influence of excited vibrational modes on this value has been considered, this value is expected to be a significant source of error regarding the evaluated concentrations.

The expression for the population difference factor includes the statistical weight factor g_I as given in (11). The neglected effect of *l*-type doubling implies errors in this factor since the rotational levels within the degenerated vibrational states are considered doubly degenerated with a statistical weight equal to 4 instead of as two separate components of statistical weights 1 and 3. The simulated spectral contributions from resonant transitions within the doubly degenerated vibrational modes therefore imply spectral lines of acetylene of too high intensity. Thus, neglecting the *l*-type doubling, will pose errors in the evaluated acetylene concentrations. The measurements performed here were carried out at room temperature. At this low temperature, however, about 85% of the molecules are in the non-degenerated vibrational ground state, for which reason errors due to *l*-type splitting of rota-

tional levels within degenerated vibrational states will be of minor importance.

As discussed in the previous section, the present *J*-dependence of the Raman linewidth models for pure acetylene has to be considered as very approximate. Since the same models are used for all mixtures, that is no influence of perturbing nitrogen molecules is included in the models, the values of the Raman linewidths may be a significant source of error. However, the fact that there are only small differences between the results obtained for the two different linewidth models, and especially that the highest accuracy is obtained for the lowest acetylene concentrations (when the acetylene rotational lines are most perturbed by the nitrogen molecules) indicates that the dominant source of error is not the Raman linewidths but the value of the polarizability anisotropy.

The simultaneously evaluated temperatures presented in Fig. 12 show an almost perfect agreement with the temperature prevailing in the laboratory for the lowest acetylene mole fraction for both linewidth models used. This is not surprising, since this spectrum consists almost entirely of rotational lines from nitrogen (see Fig. 7a), and the theoretical model for pure nitrogen is well developed and provides high temperature accuracy [13]. The results for the six other mixtures show an increasing error for increasing acetylene mole fraction when linewidth model A was used. The results using model B show a similar trend, except for the two highest acetylene concentrations (28.5% and 31.7%) for which the errors are smaller than for the fifth data point (25% acetylene). As can be seen in Fig. 7c the rotational CARS spectrum recorded in the mixture consisting of 31.7% acetylene is dominated by rotational lines of acetylene, and since the temperature evaluated from a pure acetylene spectrum using linewidth model B is in good agreement with the temperature measured by the thermocouples (see Fig. 8) it might explain the lower temperature error for the two highest acetylene concentrations using linewidth model B. This behaviour may be explained by errors in the Raman linewidths due to perturbing nitrogen molecules, since such errors are expected to induce the largest temperature errors for mixtures that results in rotational CARS spectra for which the strengths of the acetylene and nitrogen lines are comparable. It is, however, difficult to attribute the temperature errors to any isolated parameter since the spectral synthesis is very complicated. The results, however, clearly show that the Raman linewidth models used here result in different temperatures, and a deeper knowledge in the effects of nitrogen perturbation of the Raman linewidths of acetylene will certainly improve the technique for temperature measurements in acetylene/nitrogen mixtures.

Regarding the evaluated values of the non-resonant susceptibility (see Fig. 13), it is interesting to note that the evaluated values are, for both linewidth models used, almost perfectly linearly dependent on the acetylene mole fraction, with a constant of proportionality close to the calculated value, for the four lowest mole fractions. This indicates that the non-resonant susceptibility really scales to the relative concentration of the contributing species.

6 Summary

Dual-broadband rotational CARS measurements have been carried out in pure acetylene at different temperatures in the regime 294–582 K, and in different acetylene/nitrogen mixtures in the mole fraction range 0.06–0.32 for acetylene at room temperature. The spectra were evaluated using two different models for the rotational Raman linewidths, one with and one without *J*-dependence. It was found that the *J*-dependent linewidth model provides highest accuracy both regarding temperature and relative acetylene concentrations, which were generally less than 2% for the measured temperatures and less than 13% (on a relative scale) for the evaluated acetylene concentrations. Besides giving an improved quality of the spectral fits, fitting the value of the non-resonant susceptibility was found to be necessary in order to achieve high temperature accuracy. The results indicate that fitting of the non-resonant susceptibility may compensate at least small errors, both due to uncertainties in the value of the slit width and due to the neglected *l*-type energy splitting. The present model provides evaluation of complete temperature profiles measured in acetylene diffusion flames, and the results show a good potential for local measurements of acetylene/air equivalence ratios, especially at the lower temperatures prevailing in the mixing and precombustion zones, of combustion processes. However, before quantitative measurements of acetylene/air equivalence ratios can be performed, investigations of spectra that beside contributions from acetylene and nitrogen also contain oxygen contribution have to be analyzed, and such a study is planned by our group.

Acknowledgements. The authors gratefully acknowledge the experimental contributions and the introductory spectral analysis by Maria Scharin. The stimulating discussions with Christian Brackmann are also acknowledged. The work was financially supported by the Swedish National Board for Industrial and Technological Development (NUTEK), the Swedish Research Council for Engineering Sciences (TFR), and AB Sydkraft.

References

1. D.A. Greenhalgh: In *Advances in Non-linear Spectroscopy*, ed. by R.J.H. Clark, R.E. Hester (Wiley, New York 1988) p. 193
2. W. Stricker, W. Meier: In *Trends in Applied Spectroscopy* (Research Trends, Trivandrum, India 1993) p. 231
3. A.C. Eckbreth: *Laser Diagnostics for Combustion Temperature and Species* (Gordon and Breach, Amsterdam 1996)
4. R.L. Farrow, R.P. Lucht, W.L. Flower, R.E. Palmer: In Proc. 20th Symp. (Int'l) on Combustion (The Combustion Institute, Pittsburgh, PA 1984) p. 1307
5. R.P. Lucht, R.L. Farrow, R.E. Palmer: Combust. Sci. Technol. **45**, 261 (1986)
6. K. Aron, L.E. Harris, J. Fendell: Appl. Opt. **22**, 3604 (1983)
7. K.W. Boyack, P.O. Hedman: In Proc. 23rd Symp. (Int'l) on Combustion (The Combustion Institute, Pittsburgh, PA 1990) p. 1893
8. R.L. Farrow, P.L. Mattern, L.A. Rahn: Appl. Opt. **21**, 3119 (1982)
9. R.L. Farrow, R.P. Lucht, R.E. Palmer, G.L. Clark: Appl. Opt. **24**, 2241 (1985)
10. A.C. Eckbreth, T.J. Anderson: Appl. Opt. **24**, 2731 (1985)
11. R.R. Antcliff, O. Jarett, Jr.: Rev. Sci. Instrum. **58**, 2075 (1987)
12. R.P. Lucht: Opt. Lett **12**, 78 (1987)
13. L. Martinsson, P.-E. Bengtsson, M. Aldén, S. Kröll, J. Bonamy: J. Chem. Phys. **99**, 2466 (1993)
14. J. Bood, P.-E. Bengtsson, M. Aldén: ASME-paper No. 99-GT-114 (The American Society of Mechanical Engineers New York 1999)
15. L. Martinsson, P.-E. Bengtsson, M. Aldén, S. Kröll: In *Temperature: Its Measurements and Control in Science and Industry*, Vol. 6, ed. by J.F. Schooley (AIP, New York 1992) p. 679
16. P.-E. Bengtsson, L. Martinsson, M. Aldén, S. Kröll: Combust. Sci. Technol. **81**, 129 (1992)
17. P.-E. Bengtsson, M. Aldén, S. Kröll, D. Nilsson: Combust. Flame **82**, 199 (1990)
18. A.C. Eckbreth, T.J. Anderson: Opt. Lett. **11**, 496 (1986)

19. M. Aldén, P.-E. Bengtsson, H. Edner: Appl. Opt. **25**, 4493 (1986)
20. P.-E. Bengtsson, L. Martinsson, M. Aldén, B. Johansson, B. Lassesson, K. Marforio, G. Lundholm: In Proc 25th Symp. on Combustion (The Combustion Institute, Pittsburgh, PA 1994) p. 1735
21. J. Bood, P.-E. Bengtsson, F. Mauss, K. Burgdorf, I. Denbratt: SAE Paper No. 971669 (The Society of Automotive Engineers, Warrendale, PA 1997)
22. A. Leipertz, T. Seeger, H. Spiegel, E. Magens: In *Temperature: Its Measurements and Control in Science and Industry*, Vol. 5, ed. by J.F. Schooley (AIP, New York 1992) p. 661
23. A. Leipertz, E. Magens, T. Seeger, H. Spiegel: In Proc. IUTAM Symposium on Aerothermodynamics in Combustors, ed. by R.S.L. Lee, J.H. Whitelaw, T.S. Wung (Springer, Berlin, Heidelberg 1992) p. 105
24. L. Martinsson, P.-E. Bengtsson, M. Aldén: Appl. Phys. B **62**, 29 (1996)
25. T. Seeger, A. Leipertz: Appl. Opt. **35**, 2665 (1996)
26. A. Thumann, M. Schenk, J. Jonuscheit, T. Seeger, A. Leipertz: Appl. Opt. **36**, 3500 (1997)
27. J.D. Black, C.A. Long: Appl. Opt. **31**, 4291 (1992)
28. E. Magens: PhD thesis, Lehrstuhl für Technische Thermodynamik, Universität Erlangen-Nürnberg (1993)
29. M. Schenk, T. Seeger, A. Leipertz: In Proc. 16th Int. Conf. on Raman Spectroscopy, ed. by A.M. Heyns (Wiley, New York 1998) p. 160
30. P.-E. Bengtsson, L. Martinsson, M. Aldén: Appl. Spectrosc. **49**, 188 (1995)
31. H.G.M. Edwards: Spectrochemica Acta 46A, 97 (1990)
32. Y. Kabbadj, M. Herman, G. Di Lonardo, L. Fusina, J.W.C. Johns: J. Mol. Spect. **150**, 535 (1991)
33. G. Herzberg: *Molecular Spectra and Molecular Structure, Volume II. Infrared and Raman Spectra of Polyatomic Molecules*, Reprint edn. (Krieger, Florida 1991)
34. B.C. Smith, J.S. Winn: J. Chem. Phys. **89**, 4638 (1988)
35. E. Kostyk, H.L. Welsh: Can. J. Phys. **58**, 534 (1980)
36. T. Lundeen, S.-Y. Hou, J.W. Nibler: J. Chem. Phys. **79**, 6301 (1983)
37. M.P. Boogard, A.D. Buckingham, R.K. Pierens, A.H. White: J. Chem. Soc., Faraday Trans. 1 **74**, 3008 (1978)
38. I.-Y. Wang, A. Weber: Indian J. Pure Appl. Phys. **16**, 358 (1977)
39. A.C. Eckbreth: Appl. Phys. Lett. **32**, 421 (1978)
40. S. Kröll, M. Aldén, P.-E. Bengtsson, C. Löfström: Appl. Phys. B **49**, 445 (1989)
41. R.J. Hall: Combust. Flame **35**, 47 (1979)
42. R.J. Hall, J.F. Verdieck, A.C. Eckbreth: Opt. Commun. **35**, 69 (1980)
43. T. Parameswaran, D.R. Snelling: Technical Note 81-18 (Defence Research Establishment Ottawa 1982)
44. R.J. Hall, L.R. Boedeker: Appl. Opt. **23**, 1340 (1984)
45. D. Nilsson: Master's thesis (LRAP-76), Dep. of Atomic Physics, Lund Institute of Technology (1987)
46. M. Aldén, P.-E. Bengtsson, H. Edner, S. Kröll, D. Nilsson: Appl. Opt. **28**, 3206 (1989) and Erratum: Appl. Opt. **29**, 4434 (1990)
47. M.C. Drake, C. Asawaroengchai, G.M. Rosenblatt: Am. Chem. Soc. Symp. Ser. **134**, 231 (1980)
48. M.C. Drake: Opt. Lett. **7**, 440 (1982)
49. G. Placzek, E. Teller: Z. Phys. **81**, 209 (1933)
50. T.C. James, W. Klemperer: J. Chem. Phys. **31**, 130 (1959)
51. C. Asawaroengchai, G.M. Rosenblatt: J. Chem. Phys. **72**, 2664 (1980)
52. H. Kataoka, S. Maeda, C. Hirose: Appl. Spectrosc. **36**, 565 (1982)
53. R.E. Teets: Opt. Lett. **9**, 226 (1984)
54. D.A. Greenhalgh, R.L. Hall: Opt. Commun. **57**, 125 (1986)
55. F.Y. Yueh, E.J. Beiting: Comput. Phys. Commun. **42**, 65 (1986)
56. W.H. Press, B.P. Flannery, S.A. Teukolsky, W.T. Vetterling: *Numerical Recipes* (FORTRAN version), (Cambridge Univ. Press, Cambridge 1989)
57. A.J. Russel, M.A. Spackman: Mol. Phys. **88**, 1109 (1996)
58. P. Varanasi, B.R.P. Bangaru: J. Quant. Spectrosc. Radiat. Transfer **15**, 267 (1975)
59. J.S. Wong: J. Mol. Spec. **82**, 449 (1980)
60. Y. Ohsugi, N. Ohashi: J. Mol. Spec. **131**, 215 (1988)
61. D. Lambot, A. Oliver, G. Blanquet, J. Walrand, J.-P. Bouanich: J. Quant. Spectrosc. Radiat. Transfer **45**, 145 (1991)
62. D. Lambot, J.-C. Populaire, J. Walrand, G. Blanquet, J.-P. Bouanich: J. Mol. Spec. **165**, 1 (1994)
63. P. Varanasi, L.P. Giver, F.P.J. Valero: J. Quant. Spectrosc. Radiat. Transfer **30**, 497 (1983)
64. P. Varanasi, L.P. Giver, F.P.J. Valero: J. Quant. Spectrosc. Radiat. Transfer **30**, 505 (1983)
65. V. Malathy Devi, D.C. Benner, C.P. Rinsland, M.A.H. Smith, B.D. Sidney: J. Mol. Spec. **114**, 49 (1985)
66. W.E. Blass, V.W.L. Chin: J. Quant. Spectrosc. Radiat. Transfer **38**, 185 (1987)
67. D. Lambot, G. Blanquet, J.-P. Bouanich: J. Mol. Spec. **136**, 86 (1989)
68. V.I. Fabilinsky, B.B. Krynetsky, V.A. Kulevsky, V.A. Mishin, A.M. Prokhorov, A.D. Savel'ev, V.V. Smirnov: Opt. Commun. **20**, 389 (1977)
69. M.D. Duncan, P. Osterlin, R.L. Byer: Opt. Lett. **6**, 90 (1981)
70. D. Robert, J. Bonamy: J. Phys. (Paris) **10**, 923 (1979)
71. D.W. Marquardt: J. Soc. Indust. Appl. Math. **11**, 431 (1963)
72. G.J. Rosasco, W.S. Hurst: Phys. Rev. A **32**, 281 (1985)